The effect of Base on the Facile Hydrothermal Preparation of Highly Active IrO$_x$ Oxygen Evolution Catalysts

Jonathan Ruiz Esquius[a], David J. Morgan[a], Ioannis Spanos[b], Daniel G. Hewes,[a] Simon J. Freakley[c] and Graham J. Hutchings[a*]

[a] School of Chemistry, Cardiff Catalysis Institute, Cardiff University, Main Building, Park Place, Cardiff CF10 3AT, UK.

[b] Department of Heterogeneous Reactions, Max Planck Institute for Chemical Energy Conversion, Stiftstrasse 34-36, Muelheim an der Ruhr, 45470, Germany.

[c] Department of Chemistry, University of Bath, Claverton Down, Bath, BA2 2AY, UK.

* Hutch@cardiff.ac.uk

Abstract

The efficient electrochemical splitting of water is limited by the anodic oxygen evolution reaction (OER). IrO$_2$ is a potential catalyst with sufficient activity and stability in acidic conditions to be applied in water electrolysers. The redox properties and structural flexibility of amorphous iridium oxo-hydroxide compared to crystalline rutile-IrO$_2$ is associated with higher catalytic activity for OER. We prepared IrO$_x$ OER catalysts by a simple hydrothermal method varying the alkali metal base (Li$_2$CO$_3$, LiOH, Na$_2$CO$_3$, NaOH, K$_2$CO$_3$, KOH) employed during the synthesis. This work reveals that the surface area, particle morphology and the concentration of surface hydroxyl groups can be controlled by the base used, and thus, greatly influence the catalyst activity and stability for OER. It was found that materials prepared with bases containing lithium cations can lead to amorphous IrO$_x$ materials with a significantly lower overpotential (100 mV @ 1.5 mA·cm^{-2}) and increased stability compared to materials prepared with other bases and rutile IrO$_2$. This facile method leads to the synthesis of highly active and stable catalysts which can potentially be applied to larger scale catalyst preparations.

Keywords: electrocatalysis, oxygen evolution reaction, iridium oxide, amorphous iridium oxo-hydroxide, hydrothermal synthesis.

Introduction

To achieve transition from finite fossil fuel resources[1] to a hydrogen driven energy economy, surplus renewable energy needs to be converted to hydrogen and oxygen via electrolysis.[2] While H$_2$ can be efficiently produced over Pd or Pt catalysts with minimal energy losses,[3] O$_2$ evolution is composed of multiple electron transfer reactions typically leading to a higher

reaction overpotential than the thermodynamic value of 1.23 V_{RHE}. On operating cells potentials between 1.8 V_{RHE} and 2.6 V_{RHE} are reported, which corresponds to an energy loss between 31.7 % to 53 %.[4] In acid media the most studied catalysts are RuO_2 or IrO_2[5] and whilst the former is highly active it corrodes through RuO_4 formation,[6] thus iridium oxide is potentially the only feasible single oxide candidate.

Key structural features of highly active IrO_2 materials have been identified in the literature. Fierro *et al.*[7] through O^{18} isotopically labelled IrO_2 and H_2O, confirmed that active oxygen species can migrate through the IrO_2 lattice. Therefore, suggesting that IrO_2 with flexible structures, which would facilitate oxygen mobility, should outperform structurally rigid rutile IrO_2.[8, 9] Pfeifer *et al.*[10, 11] characterised commercially available amorphous IrO_x and crystalline rutile IrO_2 from Premion-Alfa Aesar and Sigma Aldrich respectively by quasi in-situ X-ray photoemission spectroscopy and near edge - X-ray absorption spectroscopy. They proposed and characterised electrophilic O^- species, which were mobile within the oxide lattice and highly susceptible to nucleophilic attack on the highly active amorphous catalyst while only lattice O^{2-} sites were detected on the less reactive rutile oxide. In a separate study performed on the same commercially available IrO_2 materials, by combining X-ray photoemission spectroscopy and density functional theory the origin of electrophilic O^- species was correlated to the presence of Ir^{III} sites, which were induced through the formation of cationic vacancies within the IrO_2 framework.[12]

To prepare highly active and stable IrO_2 catalysts a wide variety of preparation methodologies have been developed. For instance, Massue *et al.*[13] prepared 30 wt. % amorphous oxo-hydroxide IrO_2/ATO catalysts through a microwave assisted hydrothermal method. At 1.58 V_{RHE} the fresh catalysts presented a current density of 0.7 $A \cdot mg_{Ir}^{-1}$. After annealing in air at 250 °C and at 350 °C the current density dropped to 0.5 $A \cdot mg_{Ir}^{-1}$ and 0.2 $A \cdot mg_{Ir}^{-1}$ respectively due to the crystallisation of the IrO_2 and loss of active surface. Bernicke *et al.*[14] prepared iridium acetate films on Ti cylinders through a evaporation-induced self-assembly (EISA) process using poly(ethylene oxide) and poly(butadiene) as the polymer template. Annealing at 375 °C was required to completely remove the polymer and to decompose the iridium precursor to IrO_x, the highest OER activity was recorded after annealing at this temperature, whereas further increasing the annealing temperature followed by a decrease in the activity due to the progressive crystallisation of IrO_x. A similar activity trend with calcination temperature was observed for non-template iridium acetate films prepared by Reier *et at.,*[15] [15] the measured potential was close to 1.49 V_{RHE} at 0.5 $mA \cdot cm^{-2}$ for disordered films annealed at 350 °C, nevertheless, the potential increased progressively to 1.53 V_{RHE} and 1.58 V_{RHE} with increasing the calcination temperature to 450 °C and 550 °C respectively. Through XRD and XPS characterisation, the decrease in activity was related with higher crystallinity. Abbot *et*

al.[16] prepared IrO_2 catalysts via a modified Adams fusion method with a surface area of 150 $m^2 \cdot g^{-1}$ and 86 $m^2 \cdot g^{-1}$ by annealing at 350 °C or 600 °C respectively. The IrO_2 catalyst annealed at 350 °C showed lower overpotential (60 mV @ 10 $A \cdot g_{cat}^{-1}$) compared to the catalyst annealing at 600 °C, improved catalytic activity was correlated to the lower crystallinity of the former catalyst instead of to its higher surface area. Similar results on IrO_2 catalysts prepared by the Adams fusion method were observed by Felix *et al.*,[17] calcination above 350 °C induced catalyst crystallisation with the concomitant activity drop.

The synthesis of amorphous iridium oxo-hydroxides at low temperature to minimise IrO_2 crystallisation is desired to ensure key catalytic features; structural flexibility, presence of O^- species and Ir^{III} sites. Heat treatment on dried IrO_x samples can be avoided through a hydrothermal synthesis. Under strong alkaline conditions aqueous solutions of iridium salts hydrolyse and condense forming first Ir-O-oligomers followed by stable IrO_x colloidal suspensions without the need for organic stabilising ligands,[18] precipitation can be induced by heating the solution to reflux to obtain IrO_x solid. Typically, NaOH or KOH bases are widely used.[13, 19-28] More recently, amorphous IrO_x prepared with LiOH produced a catalyst with low overpotential (270 mV @ 10 $mA \cdot cm^{-2}$) and stable activity for 10 h.[9] Berkerman briefly studied the effect of the base on the stability of IrO_x colloidal suspensions, where limited differences were observed in the nature of the colloidal suspension, however, the colloidal suspensions were not assessed for OER.[29] Apart from the work of Berkerman, no reference to effect of the base employed in the hydrothermal synthesis of IrOx powders has been reported in the literature. We therefore now present a study showing that the physicochemical proprieties of amorphous hydrothermally prepared IrO_x materials can be tailored by the base used (LiOH, NaOH, KOH, Li_2CO_3, Na_2CO_3, K_2CO_3) and determine its effect towards the OER performance in terms of OER activity and stability under acidic conditions.

Experimental

Materials

All chemicals were purchased from commercial suppliers and used as received. Iridium chloride hydrate ($IrCl_3 \cdot xH_2O$ 99 %, Sigma Aldrich), rutile IrO_2 (99.9 % metal basis, Sigma Aldrich), $IrO_x \cdot$hydrate (99.99 % metal basis, Premion®, AlfaAesar), LiOH (98 %, Sigma Aldrich), Li_2CO_3 (99 %, Fisher Chemicals), Na_2CO_3 (99.5 %, Fisher Chemicals), K_2CO_3 (99 %, Fisher Chemicals), NaOH (99.6 %, Fisher Chemicals), KOH (95 %, Fisher Chemicals), perchloric acid, ($HClO_4$ 70 % in water, Honeywell Fluka), 5 % Perfluorinated resin solution (Nafion® solution, Sigma Aldrich), Ethanol (100 %, VWR Chemicals).

Catalyst Synthesis

A modification of the hydrothermal method reported by Reetz and Feigel[29] was followed. 1 mmol of $IrCl_3$ hydrate and 8 mmol of base (Li_2CO_3, LiOH, Na_2CO_3, NaOH, K_2CO_3 or KOH) were dissolved in 10 ml of deionised water and stirred for 16 h at room temperature in a 50 ml round bottom flask. The pH of the solution remained between 11-12 during this process. The solution remained yellow when carbonate bases (Li_2CO_3, Na_2CO_3 or K_2CO_3) were used, while blue solutions were generated when hydroxide bases were used (LiOH, NaOH or KOH). A further 10 ml of deionised water were added to the solution after this initial period. The solution was then heated to reflux for 3 hours. A blue precipitate was observed which was recovered by filtration and washed with 2 L of hot deionised water. Finally, the material was left to dry at room temperature for 16 h. Samples are denoted as IrO_x-(base), for example, the sample prepared using Li_2CO_3 as a base is referred as IrO_x-Li_2CO_3.

Catalyst characterisation

Powder X-ray diffraction (XRD) were performed on a X'PertPro Panalytical instrument fitted with a hemispherical analyser using a Cu Kα (1.54 Å, 40 eV) X-ray source with a Ni filter. BET surface areas were obtained on a Micromeritics 3-flex, prior to analysis the materials were dehydrated in static air at 130 °C for 20 h, then were transferred to the BET bulb and dried under vacuum at 130 °C for 16 h. Raman spectroscopy was carried out in a Renishaw InVia Raman spectrometer using a 514 nm laser with 25 mW power and a beam diameter of 0.65 nm, data acquisition was performed at 5 % laser intensity, 500 accumulations and 5 s of exposure time. X-ray photoelectron spectroscopy (XPS) were recorded on a Thermo Scientific K-Alpha+ spectrometer equipped with an Al source operating at 72 W (6 mA x 12 kV) with 20 eV pass energy, data was analysed using Casa XPS software. Scanning electron microscopy with energy dispersive X-ray spectroscopy (SEM-EDX) images were obtained on a Tescan Maia 3 microscope. The $IrCl_3$ conversion to IrO_x was monitored using UV-Vis spectroscopy in a Cary UV 60 Agilent Technologies spectrophotometer. To facilitate sampling, the hydrothermal preparation was carried out in a 100 ml 3-neck round bottom flask with 40 ml of deionised water, a reflux condenser was attached on one neck, while the other two were sealed with a rubber septum. Before sampling, the reaction temperature was allowed to stabilise for 5 min, then 0.1 ml of reaction aliquot was diluted in a UV cuvette with deionised water to 2 ml. The concentration of lithium in prepared samples was analysed by inductively coupled plasma (ICP) in an Agilent 7900 instrument after acid digestion.

Catalyst testing

To prepare the catalyst ink, 5 mg of catalyst were re-dispersed on 1.23 mL of water, 1.23 mL of ethanol and 40 µl of nafion solution. The mixture was sonicated for 30 min in order to ensure the complete re-dispersion of the material. 10 µl of the catalyst ink was drop-cast onto the working electrode and dried under a N_2 flow for 30 min to obtain a catalyst loading of 100 µg·cm^{-2}.

Electrochemical measurements were recorded on a 3-electrode flow cell reactor described previously in the literature.[30] Using a Col-Parmer Masterflex C/L single channel pump 1.2 ml·min^{-1} of 0.1 M $HClO_4$ electrolyte solution passed through the reactor, the electrolyte solution was degassed with N_2 for 30 minutes prior to reaction. A coiled Pt wire (127 µm diameter, 99.99 %, Sigma Aldrich) was used as counter electrode, a glassy carbon (0.196 cm^2)[30] was used as the working electrode and a calomel electrode ([Cl$^-$/Hg$_2$Cl$_2$/Hg/Pt], IJ Cambria Scientific Ltd, model CHI-150) as the reference. The catalyst activity towards OER was measured by linear sweep voltammetry (LSV, 1.2 V_{RHE} to 1.7 V_{RHE} at 5 mV·s^{-1}) and the catalysts stability was assessed by chronopotentiometry (CP, 2 h at 10 mA·cm^{-2}). Reported results are expressed against the reversible hydrogen electrode (RHE).

Results and discussion

Effect of Base on IrO$_x$ Morphological and Structural Properties

Under strong aqueous alkaline conditions $IrCl_3$ is converted to IrO_x following the mechanism proposed in equations 1-3.[28] The chemical conversion of $IrCl_3$ can be monitored by UV-vis spectroscopy since the reaction intermediates $Ir(H_2O)_3Cl_3$, $[Ir(OH)_6]^{3-}$ and Ir_nO_m oligomers present absorption bands at 400 nm, 320 nm and 580 nm respectively.[28]

$$Ir(H_2O)_3Cl_3 + 6\ OH^- \rightarrow [Ir(OH)_6]^{3-} + 3\ Cl^- + 3\ H_2O \qquad \text{Eq. 1}$$

$$n\ [Ir(OH)_6]^{3-} \rightarrow Ir_nO_m + m\ H_2O + 6n\ OH^- \qquad \text{Eq. 2}$$

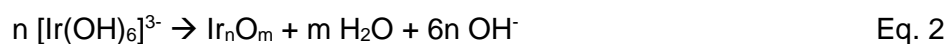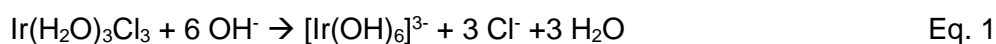$$Ir_nO_m + O_2 \rightarrow n\ IrO_2 \qquad \text{Eq. 3}$$

Figure 1 shows the UV-vis spectra acquired during the preparation of IrO_x-LiOH and IrO_x-Li_2CO_3 (UV-vis spectra for remaining catalysts available in Figure S1). When using Li_2CO_3, $IrCl_3$·$3H_2O$ hydrolysed to $[Ir(OH)_6]^{3-}$ after 16 h at 25 °C as indicated by the gradual decrease in intensity at 400 nm corresponding to $Ir(H_2O)_3Cl_3$ and the formation of the band at 320 nm indicating the formation of $[Ir(OH)_6]^{3-}$. To induce the formation of Ir-O-Ir linkages or Ir-oxy oligomers, giving rise to a characteristic absorption band at 580 nm, heating to 85-95 °C was required, with no IrO_x precipitation observed prior to reaching reflux. After 30 minutes of reflux,

no absorption bands were observed indicating the absence of iridium species in solution and full precipitation of the IrO_x material. In contrast, the strong nature of LiOH and its increased solubility compared to its carbonate counterpart[31] resulted in faster reaction kinetics. After stirring at 25 °C for 16 h, the presence of $[Ir(OH)_6]^{3-}$ and Ir_nO_m were detected at 320 nm and 580 nm respectively without heating or reflux. Heating induced the further polymerisation of Ir-oxy oligomers and the precipitation of IrO_x. Nevertheless, even though IrO_x precipitated during reflux, $[Ir(OH)_6]^{3-}$ remained in solution as observed by the band at 320 mn, indicating its incomplete precipitation or re-dissolution under strongly alkaline conditions. The observations were consistent between carbonates and hydroxides with differing cations suggesting that the nature of the anions and base strength control the kinetics of the IrO_x formation.

To detect the presence of any crystalline phases, materials were characterised by XRD. Commercially available amorphous IrO_x·(IrO_x-AA) and rutile IrO_2 (IrO_2-SA) from Premion-Alfa Aesar and Sigma Aldrich, which has been thoroughly characterised in the literature[10-12, 32] were used as standards. In agreement with previous reports, rutile (JCPDS-015-0876) and metallic iridium (JCPDS-006-0598) impurity were observed by XRD for the respective crystalline and amorphous commercial samples (Figure S2). The absence of a defined diffraction pattern and broad reflections at 34° suggested an amorphous nature of all hydrothermally prepared IrO_x materials regardless of the base used (Figure 2). In addition the presence of metallic Ir was not detected in any samples due to the absence of reducing agents or high temperature treatments in the preparation method, which are commonly used in IrO_x synthesis, reported in the literature.[8, 13-16, 28, 33] The IrO_x materials were additionally analysed by Raman spectroscopy (Figure S3) to detect any presence of the A_{1g} and E_g modes at 752 cm^{-1} and 561 cm^{-1} characteristic of rutile IrO_2 which were observed on the crystalline commercial sample.[34-36] No distinct absorption bands were detected for the amorphous commercial sample or for the hydrothermally prepared IrO_x samples, confirming the absence of any rutile crystalline phases.

The morphology, surface roughness and pore structure of materials influence the O_2 bubble formation and detachment during reaction which can greatly alter the catalyst performance by controlling diffusion properties.[4] Slow gas bubbles detachment can translate in electrode/electrolyte mass transport limitations accounting to higher overpotential and high ohmic voltage drop. Generally smooth samples, without characteristic structural features at the surface such as cracks or pores, are limited by slow bubble detachment compromising the stability of the electrode.[14, 37] The macroscopic morphology of IrO_x materials prepared with different bases was studied by SEM and is presented in Figure 3. For the materials

synthesised it was observed that, the final morphology was highly influenced by the base used, with the alkali metal cation of the base seemingly influencing the IrO_x precipitation process towards specific morphologies. Both IrO_x-KOH and IrO_x-K_2CO_3 presented large aggregates with flat surfaces, similar to the commercial crystalline sample. Whereas IrO_x-LiOH and IrO_x-Li_2CO_3 precipitated with a sponge-like morphology, resembling the commercial amorphous IrO_x-AA material. An intermediate picture with flat surfaces and sponge-like areas was observed for IrO_x-NaOH and IrO_x-Na_2CO_3 catalysts. Apart from the differences evident in the morphology EDX was used to determine the presence of impurities in the materials. No significant chloride contamination was detected on any of the synthesised catalysts at the detection limits of the instrument (0.1 at. %), in agreement with XPS characterisation. In IrO_x samples prepared with sodium or potassium bases *ca.* 2 at.% of the corresponding alkali metal cation could be detected in each case. In IrO_x-Li_2CO_3 and IrO_x-LiOH materials the concentration of lithium could not be determined by EDX because of its low atomic mass. Lithium concentration was determined by ICP through acid digestion in aqua regia to $3 \cdot 10^{-3}$ at. %, which is significantly lower compared to sodium and potassium observed for the previous catalysts by EDX.

Catalysts prepared using K or Na-containing bases showed very low N_2-BET surface areas, typically < 5 $m^2 \cdot g^{-1}$, comparable to the commercial rutile IrO_2. However, the sponge-like morphology observed for Li-based catalysts can be correlated with an increased surface area. The surface area of IrO_x-Li_2CO_3 catalyst is comparable to the commercially sourced IrO_x-AA of 32 $m^2 \cdot g^{-1}$ (Table 1). High surface area materials are desired since it allows an increase in the concentration of active sites in contact with the reaction media and increased mass transport properties, however many studies have shown that IrO_2 activity towards OER is in general not linearly correlated with the surface area.[38] However due to the synthesised materials having comparable surface areas to the commercial standards factors controlling activity and stability other than surface area can be identified. Massue *et al.*[19] reported that varying the $IrCl_3$ to KOH molar ratio during the hydrothermal preparation of IrO_x materials the surface area can be tailored from 150 $m^2 \cdot g^{-1}$ to 2 $m^2 \cdot g^{-1}$, nevertheless, no correlation between the surface area and the catalytic activity towards OER was found. In conclusion, the catalyst's activity was assigned to a contribution of the nature of the hydroxyl groups, the presence of Ir^{III} and Ir^{IV} sites and to the existence of electrophilic O^- species.

XPS characterisation was used to assess the catalysts surface composition. Ir(4f) and O(1s) core-levels for single crystal rutile IrO_2 have been shown to be asymmetric as a result of its conductive metallic-like properties.[39] However, normal fitting parameters used for metallic samples are not suitable for IrO_2,[40] making the Ir(4f) orbital speciation challenging due to

combined influence of band structure (4f and 5p),[32] electron correlation and spin-orbit coupling on the electronic structure.[40, 41] Pfeifer et $al.$[11, 12] performed rigorous synchrotron-based XPS characterisation on commercial rutile IrO_2-SA and amorphous IrO_x-AA samples, however their derived line shapes are not directly translatable to laboratory scale XPS instruments. Morgan et $al.$[32] reported the Ir(4f) and O(1s) peak fitting parameters applicable to lab-based XPS measurements for the same commercial standards utilising a Shirley background and Finite-Lorentzian and Gaussian-Lorentzian lineshapes. In agreement with published data,[32] the Ir(4f) and O(1s) peak fitting proposed for the commercial standards can be translated into our measurements (Figure 4). The asymmetric $Ir(4f_{7/2})$ and O(1s) peaks for rutile IrO_2-SA standard, were centred at 61.9 eV and 530.0 eV respectively with a Ir/O ratio of 0.49, in excellent agreement with the expected values of 0.50, indicating that it was composed exclusively of Ir^{IV} and O^{2-} lattice oxygen sites. Whilst the $Ir(4f_{7/2})$ peak for the commercial IrO_x-AA catalyst appreciably broaden and shifted upward to 62.5 eV, indicating the co-existence of Ir^{IV} and Ir^{III} sites in the oxide matrix. The Ir/O ratio decreased to 0.31 indicating a higher concentration of oxygen compared to the nominal value. Additionally, the presence of water, hydroxide groups and oxide oxygen species were detected respectively at 532.4 eV, 531.1 eV and 530.2 eV on the O(1s) orbital.[32, 42]

Applying the XPS lineshape on to the synthesised IrO_x catalysts it is evidenced that, regardless of the base used, the Ir(4f) orbital is broader and shifted towards higher binding energy compared to rutile IrO_2 (Figure S4). This can be assigned to the presence of Ir^{IV} and Ir^{III} centres as elucidated for the amorphous standard (figure 4a) albeit the concentration of each oxidation state in the material could not be deduced because of the absence of a good Ir^{III} oxide standard. In correlation with the amorphous commercial sample, for synthesised samples, the Ir/O ratio indicated an excess of oxygen compared to the stoichiometric oxide (Table S1), which would indicate the presence of chemisorbed water and surface hydroxide groups. Moreover, the O(1s) peak did not show the typical asymmetry observed for rutile IrO_2 with higher binding energy, between 530.7 eV and 531.5 eV, which can be resolved as three components: oxide, hydroxide and water/carbonate (figure 4b for IrO_x-Li_2CO_3 and Figure S5 for all IrO_x-base catalysts).

Table 2 shows the oxygen speciation obtained from the O(1s) peak deconvolution. It is noted that the proportion of oxide and hydroxide varies significantly with the base employed during the synthesis. Catalysts prepared with lithium bases, IrO_x-Li_2CO_3 and IrO_x-LiOH, have the highest proportion of hydroxide and the lowest oxide concentration, comparable to the proportion observed for the commercial IrO_x-AA material, which could be related with a higher

concentration of Ir^{III} centres in the IrO_x lattice. Whilst a more oxidic surface is observed for catalysts prepared with sodium and potassium bases.

Catalytic activity towards OER

Hydrothermally prepared IrO_x and the commercial standards (IrO_2-SA and IrO_x-AA) were tested for OER in an identical flow electrochemical reactor described previously by Spanos *et al.*[30] The intrinsic catalytic activity was determined by LSV (1.2 V_{RHE} to 1.7 V_{RHE} at 5 mV·s^{-1}). In agreement with literature,[12] commercial rutile IrO_2-SA performed poorly compared to amorphous IrO_x-AA (dashed LSV traves in figure 5) as a consequence of the absence of key structural features: electrophilic O^- sites, the presence of Ir^{III} and Ir^{IV} centres, structural flexibility and surface composition. No appreciable current density was observed for the rutile sample over the whole studied potential range, whilst the amorphous standard reached a current density of 22 mA·cm^{-2} at 1.52 V_{RHE} (figure 5). A decrease in the intrinsic catalytic activity compared to the amorphous standard was observed for IrO_x samples prepared with NaOH, Na_2CO_3, KOH or K_2CO_3 respectively. This can be correlated with the significantly lower measured surface area for these catalysts, in conjunction with the lower proportion of surface hydroxide groups and the concomitant more oxidic surface despite all material being amorphous in nature, as confirmed by XPS, and the high concentration of sodium and potassium detected by EDX which can poison catalytic active sites, as reported for IrO_x prepared with KOH as base in the literature.[19] Despite the IrO_x-LiOH material presenting one third of the surface area of the commercial amorphous standard, it showed almost identical catalytic activity to the commercial IrO_x-AA material. Thus, stressing that the nature of the active surface is dominant in determining activity towards OER rather than the surface area.[19, 38] The IrO_x-Li_2CO_3 catalyst, which showed comparable surface area, surface composition and morphology to the commercial IrO_x-AA standard, outperformed in activity by reduction of 25 mV in overpotential at 22 mA·cm^{-2}. Electrochemically active surface area (ECSA) and iridium mass normalised activities confirmed the higher activity of IrO_x-Li_2CO_3 compared to IrO_x-AA and IrO_x-LiOH (Figure S6 and Figure S7). No substantial differences in measured Tafel slopes for IrO_x-AA (37 mV·dec^{-1}), IrO_x-Li_2CO_3 (38 mV·dec^{-1}) and IrO_x-LiOH (35 mV·dec^{-1}) were observed (Figure S8). The high activity of the two samples prepared with Li^+ containing bases and different anions may suggest that a promotion in activity could be induced by residual Li^{+}[9] remaining in the structure of IrO_x materials. To prove the higher promoting effect of Li^+ compared to Na^+ and K^+, the catalyst ink of rutile IrO_2 was prepared with 1.23 ml of 0.1 M aqueous alkaline solution (LiOH, NaOH or KOH), 1.23 ml of ethanol and 40 µl of nafion. The catalytic activity for OER was assessed by LSV (Figure S9a), Li^+, Na^+ and K^+-doped rutile IrO_2 were more active than rutile IrO_2-SA, which can be attributed to the formation of surface

hydroxyl groups in the presence of base. However, Li^+-doped rutile IrO_2 outperformed in activity Na^+ and K^+-doped rutile IrO_2, in agreement with a previous study.[9] To ensure that increased activity observed in cation-doped IrO_2-SA was not only related to the formation of surface hydroxide groups, as a result of the catalyst ink preparation, an IrO_2-SA electrode was prepared in standard conditions (H_2O/ethanol/nafion). Then OER activity was measured by LSV after consecutive additions of 0.1 M LiOH (Figure S9b), after each 0.5 ml addition it is observed a progressive increase in the current density, suggesting a Li^+ promoting effect. Nevertheless, the nature of improved activity in the presence of Li^+ remains unclear and might be attributed to the formation of active structural motifs[38] or to an increase in the population of active sites.

More important than the intrinsic catalytic activity of IrO_x materials towards OER is the catalyst stability against corrosion. As a classic example, RuO_2 presents higher activity than IrO_2, nevertheless, iridium catalysts are generally desired towards OER as a consequence of its improved stability against dissolution.[5] The stability of the catalysts was determined by chronopotentiometry (CP, 2 h at 10 mA·cm^{-2}). Crystalline IrO_2 and catalysts prepared with other bases than LiOH or Li_2CO_3 showed a rapid increase in the potential to 2.2 V_{RHE} (figure 6), within the first two minutes of the CP experiment, corresponding to the glassy carbon tip corrosion, this in agreement with the limited catalytic activity observed by LSV. The IrO_x-LiOH catalyst presented an almost identical stability profile to the amorphous commercial standard with a potential increase of 170 mV during the CP experiment. Improved intrinsic activity observed for IrO_x-Li_2CO_3 catalyst by LSV translated also in enhanced stability during the CP experiment, compared to IrO_x-LiOH and the state of the art IrO_x-AA, the potential increased by only 12 mV during the two hour duration of the stability test. This corresponded to an improvement in the degradation rate of one order of magnitude compared to the amorphous standard.

To assess the extent of catalyst deactivation caused by the CP experiments (2 h at 10 mA·cm^{-2}), LSV was measured and compared at a current density of 25 mA·cm^{-2} to the initial intrinsic catalytic activity (Figure S10). For catalysts that showed corrosion of the glassy carbon electrode during CP, severe deactivation was observed since 25 mA·cm^{-2} was not reached in the second LSV experiment (change in more than 0.5 V compared to the fresh sample). The catalytic activity of IrO_2-LiOH was seriously compromised after CP, and the current density measured by LSV also did not reach 25 mA·cm^{-2}. IrO_2-Li_2CO_3 showed a potential increase of only 38 mV after CP to reach 25 mA·cm^{-2} compared to 80 mV for commercial IrO_2-AA. To elucidate the difference in stability between synthesised IrO_x-Li_2CO_3 and commercial IrO_x-AA during CP (2 h at 10 mA·cm^{-2}), iridium dissolution was simultaneously monitored during CP

by coupling an ICP to the flow cell set up, as described previously in literature.[30] Note that for this experiment, the electrode used was made of gold instead of glassy carbon, since gold substrates shows better cohesion with the catalysts[43, 44], which would prevent iridium dissolution because of IrO_x detachment as opposed to iridium corrosion produced during OER. As shown in figure 7a, and in agreement with previously published data, iridium corrosion was detected for commercial IrO_x-AA during the first 30 minutes of CP,[30] which is related with the increase in the LSV potential observed when comparing measurements before and after CP (Figure 7b). Whilst no significant corrosion was detected for IrO_x-Li_2CO_3 during CP (Figure 7a), in accordance with no catalytic deactivation observed on consecutive LSV measurements (Figure 7b). These results suggest that the IrO_x-Li_2CO_3 materials is a highly active and stable catalyst that is easily prepared and could be used as a standard for future mechanistic studies.

Conclusions

Amorphous iridium oxo-hydroxides catalysts can be successfully prepared through a facile hydrothermal method in alkaline conditions, the base used during the synthesis is important in tailoring the physico-chemical proprieties of OER catalysts. Regardless of the base, no crystalline phase contamination, rutile or metallic iridium, were detected by XRD. However, the cation present (Li^+, Na^+ or K^+) seems to strongly effect the final morphology of the material while the anion effects the rate of the condensation steps during the preparation. IrO_x catalysts prepared with LiOH or Li_2CO_3 showed a porous sponge-like morphology with higher surface area than catalysts prepared with Na^+ or K^+ containing bases. XPS characterisation showed a Ir(4f) orbital shift and broadening when compared to rutile IrO_2 for all prepared samples, indicating the presence of Ir^{III} and Ir^{IV} sites, independently of the base used during the synthesis. The Ir/O ratio indicated an excess of oxygen compared to the stoichiometry for rutile IrO_2. Additionally, apart from the oxide lattice oxygen, the O(1s) region indicated the presence of hydroxide groups and water. O(1s) peak deconvolution indicated that IrO_x catalyst prepared with LiOH or Li_2CO_3 as a base have a higher concentration of hydroxide groups at the surface compared to catalysts prepared with Na or K bases. The surface area dictated from the observed morphology could not be directly related with the intrinsic catalytic activity towards OER. Conversely, catalysts with the higher proportion of oxide showed limited activity by LSV and poor stability by CP towards OER, whilst catalysts with the higher concentration of hydroxide groups and the least oxide nature outperformed in activity and stability. While IrO_x prepared with Li_3CO_3 showed a reduced overpotential of 25 mV at 22 mA·cm^{-2} and an order of magnitude improvement in the catalyst stability at 10 mA·cm^{-2} than a commercial standard (amorphous IrO_2 from Alfa Aesar) with similar morphology, surface area and surface composition. This could suggest a promotional role of the alkali metal ions that remain in the

material after preparation, particularly Li^+, which could play a role in producing active and stable IrO_x catalysts.

Associated content

Support Information Available: UV-Vis monitoring of the $IrCl_3$ conversion to IrO_x in the presence of NaOH, Na_2CO_3, KOH and K_2CO_3; XRD patterns of commercial IrO_2-SA and IrO_x-AA; Raman spectroscopy; Ir(4f), O(1s) and Ir:O ratio obtained by XPS for synthesised IrO_x catalysts; ECSA and Ir-mass normalised activities for IrO_x-Li_2CO_3, IrO_x-LiOH and IrO_x-AA; Tafel slopes for IrO_x-Li_2CO_3, IrO_x-LiOH and IrO_x-AA; Li^+, Na^+ and K^+-doped rutile IrO_2-SA; Increase in the reaction potential by LSV after CP stability test.

Acknowledgements

References

1. Rockstrom, J.; Steffen, W.; Noone, K.; Persson, A.; Chapin, F. S.; Lambin, E. F.; Lenton, T. M.; Scheffer, M.; Folke, C.; Schellnhuber, H. J.; Nykvist, B.; Wit, C. A.; Hughes, T.; Leeuw, S.; Rodhe, H.; Sörlin, S.; Snyder, P. K.; Costanza, R.; Svedin, U.; Falkenmark, M.; Karlberg, L.; Corell, R. W.; Fabry, V. J.; Hansen, J.; Walker, B.; Liverman, D.; Richardson, K.; Crutzen, P.; Foley, J. A. A safe operating space for humanity, *Nature*, **2009**, *461* (7263), 472-475.

2. Schlögl, R. The Role of Chemistry in the Energy Challenge, *ChemSusChem*, **2010**, *3* (2), 209-222.

3. Norskov, J. K.; Christensen, C. H. Toward Efficient Hydrogen Production at Surfaces, *Science*, **2006**, *312* (5778), 1322-1323.

4. Wang, M.; Wang, Z.; Gong, X.; Guo, Z. The intensification technologies to water electrolysis for hydrogen production - A review, *Renewable and Sustainable Energy Reviews*, **2014**, *29*, 573-588.

5. Carmo, M.; Fritz, D. L.; Mergel, J.; Stolten, D. A comprehensive review on PEM water electrolysis, *International Journal of Hydrogen Energy*, **2013**, *38* (12), 4901-4934.

6. Kötz, R.; Stucki, S.; Scherson, D.; Kolb, D. M. In-situ identification of RuO_4 as the corrosion product during oxygen evolution on ruthenium in acid media, *Journal of Electroanalytical Chemistry and Interfacial Electrochemistry*, **1984**, *172* (1–2), 211-219.

7. Fierro, S.; Nagel, T.; Baltruschat, H.; Comninellis, C. Investigation of the oxygen evolution reaction on Ti/IrO_2 electrodes using isotope labelling and on-line mass spectrometry, *Electrochemistry Communications*, **2007**, *9* (8), 1969-1974.

8. Tsuji, E.; Imanishi, A.; Fukui, K. I.; Nakato, Y. Electrocatalytic activity of amorphous RuO_2 electrode for oxygen evolution in an aqueous solution, *Electrochimica Acta*, **2011**, *56* (5), 2009-2016.

9. Gao, J.; Xu, C. Q.; Hung, S. F.; Liu, W.; Cait, W.; Zeng, Z.; Jia, C.; Chen, H. M.; Xiao, H.; Li, J.; Huang, Y.; Liu, B. Breaking Long-Range Order in Iridium Oxide by Alkali Ion for Efficient Water Oxidation, *Journal of the American Chemical Society*, **2019**, 141 (7), 3014-3023.

10. Pfeifer, V.; Jones, T. E.; Wrabetz, S.; Massué, C.; Velasco Velez, J. J.; Arrigo, R.; Scherzer, M.; Piccinin, S.; Hävecker, M. A. Knop-Gericke, R. Schlögl, Reactive oxygen species in iridium-based OER catalysts, *Chemical Science*, **2016**, *7* (11), 6791-6795.

11. Pfeifer, V.; Jones, T. E.; Velasco Velez, J. J.; Massué, C.; Greiner, M. T.; Arrigo, R.; Teschner, D.; Girgsdies, F.; Scherzer, M.; Allan, J.; Hashagen, M.; Weinberg, G.; Piccinin, S.; Hävecker, M.; Knop-Gericke, A.; Schlögl, R. The electronic structure of iridium oxide electrodes active in water splitting, *Physical Chemistry Chemical Physics*, **2016**, *18* (4), 2292-2296.

12. Pfeifer, V.; Jones, T. E.; Velasco Vélez, J. J.; Massué, C.; Arrigo, R.; Teschner, D.; Girgsdies, F.; Scherzer, M.; Greiner, M. T.; Allan, J.; Hashagen, M.; Weinberg, G.; Piccinin, S.; Hävecker, M.; Knop-Gericke, A.; Schlögl, R. The electronic structure of iridium and its oxides, *Surface and Interface Analysis*, **2016**, *48* (5), 261-273.

13. Massué, C.; Pfeifer, V.; Huang, X.; Noack, J.; Tarasov, A.; Cap, S.; Schlögl, R. High-performance supported Ir-oxohydroxide water oxidation electrocatalysts, *ChemSusChem*, **2017**, 10, 1943-1957.

14. Bernicke, M.; Ortel, E.; Reier, T.; Bergmann, A.; Ferreira de Araujo, J.; Strasser, P.; Kraehnert, R. Iridium Oxide Coatings with Templated Porosity as Highly Active Oxygen Evolution Catalysts: Structure-Activity Relationships, *ChemSusChem*, **2015**, *8* (11), 1908-1915.

15. Reier, T.; Teschner, D.; Lunkenbein, T.; Bergmann, A.; Selve, S.; Kraehnert, R.; Schlögl, R.; Strasser, P. Electrocatalytic Oxygen Evolution on Iridium Oxide: Uncovering Catalyst-Substrate Interactions and Active Iridium Oxide Species, *Journal of The Electrochemical Society*, **2014**, *161* (9), F876-F882.

16. Abbott, D. F.; Lebedev, D.; Waltar, K.; Povia, M.; Nachtegaal, M.; Fabbri, E.; Copéret, C.; Schmidt, T. J. Iridium oxide for the Oxygen Evolution Reaction: Correlation between particle size, morphology, and the surface hydroxo layer from operando XAS, *Chem Mater*, **2016**, *28* (18), 6591-6604.

17. Felix, C.; Maiyalagan, T.; Pasapathi, S.; Bladergroen, B.; Linkov, V. Synthesis and optimization of IrO_2 electrocatalysts by Adams fusion method for solid polymer electrolyte electrolysers., *Micro and nanosystems*, **2012**, *4*, 186-191.

18. Astruc, D. Nanoparticles and Catalysis, Wiley, **2008**.

19. Massué, C.; Huang, X.; Tarasov, A.; Ranjan, C.; Cap, S.; Schlögl, R. Microwave Assisted Synthesis of Stable and Highly Active Ir-oxohydroxides for Electrochemical Oxidation of Water, *ChemSusChem*, **2017**, 10, 1958-1968.

20. Wu, Q.; Xu, D.; Xue, N.; Liu, T.; Xiang, M.; Diao, P. Photo-catalyzed surface hydrolysis of iridium(III) ions on semiconductors: a facile method for the preparation of semiconductor/IrO_x composite photoanodes toward oxygen evolution reaction, *Phys Chem Chem Phys*, **2017**, *19* (1), 145-154.

21. Nakagawa, T.; Beasley, C. A.; Murray, R. W. Efficient Electro-Oxidation of Water near Its Reversible Potential by a Mesoporous IrO_x Nanoparticle Film, *The Journal of Physical Chemistry C*, **2009**, *113* (30), 12958-12961.

22. Zhao, Y.; Hernandez-Pagan, E. A.; Vargas-Barbosa, N. M.; Dysart, J. L.; Mallouk, T. E. A High Yield Synthesis of Ligand-Free Iridium Oxide Nanoparticles with High Electrocatalytic Activity, *The Journal of Physical Chemistry Letters*, **2011**, *2* (5), 402-406.

23. Nakagawa, T.; Bjorge, N. S.; Murray, R. W. Electrogenerated IrO_x Nanoparticles as Dissolved Redox Catalysts for Water Oxidation, *Journal of the American Chemical Society*, **2009**, *131* (43), 15578-15579.

24. Lee, S. H. A.; Zhao, Y.; Hernandez-Pagan,E. A.; Blasdel, L.; Youngblood, W. J.;Mallouk, T. E. Electron transfer kinetics in water splitting dye-sensitized solar cells based on core-shell oxide electrodes, *Faraday Discussions*, **2012**, *155*, 165-176.

25. Zhao, Y.; Vargas-Barbosa, N. M.; Strayer, M. E.; McCool, N. S.; Pandelia, M. E.; Saunders, T. P.; Swierk, J. R.; Callejas, J. F.; Jensen, L.; Mallouk, T. E. Understanding the Effect of Monomeric Iridium(III/IV) Aquo Complexes on the Photoelectrochemistry of $IrO_x \cdot nH_2O$-Catalyzed Water-Splitting Systems, *Journal of the American Chemical Society*, **2015**, *137* (27), 8749-8757.

26. Moghaddam, R. B.; Wang, C.; Sorge, J. B.; Brett, M. J.; Bergens, S. H. Easily prepared, high activity Ir-Ni oxide catalysts for water oxidation, *Electrochemistry Communications*, **2015**, *60*, 109-112.

27. Wang, C.; Moghaddam, R. B.; Bergens, S. H. Active, Simple Iridium-Copper Hydrous Oxide Electrocatalysts for Water Oxidation, *The Journal of Physical Chemistry C*, **2017**, *121* (10), 5480-5486.

28. Xu, D.; Diao, P.; Jin, T.; Wu, Q.; Liu, X.; Guo, X.; Gong, H.; Li, F.; Xiang, M.; Ronghai, Y. Iridium Oxide Nanoparticles and Iridium/Iridium Oxide Nanocomposites: Photochemical Fabrication and Application in Catalytic Reduction of 4-Nitrophenol, *ACS Applied Materials & Interfaces*, **2015**, *7* (30), 16738-16749.

29. Berkermann, F. *Preparation and Application of Aqueous Iridium Oxide Colloids* (Doctoral Thesis). Ruhr University Bochum,Germany, **2010**.

30. Spanos, I.; Auer, A. A.; Neugebauer, S.; Deng, X.; Tüysüz, H.; Schlögl, R. Standardized Benchmarking of Water Splitting Catalysts in a Combined Electrochemical Flow Cell/Inductively Coupled Plasma-Optical Emission Spectrometry (ICP-OES) Setup, *ACS Catal*, **2017**, 7, 3768-3778.

31. U.S. National Library of Medicine, PubChem (pubchem.ncbi.nlm.nih.gov).

32. Freakley, S. F.; Esquius, J. R.; Morgan, D. J. The X-ray photoelectron spectra of Ir, IrO_2 and $IrCl_3$ revisited, *Surface and Interface Analysis*, **2017**, *49* (8), 794-799.

33. Oakton, E.; Lebedev, D.; Povia, M.; Abbott, D. F.; Fabbri, E.; Dedorov, A.; Nachtegaal, M.; Copéret, C.; T. Schmidt, T. J. IrO_2-TiO_2: A high-Surface-Area, Active, and Stable Electrocatalyst for the Oxygen Evolution Reaction, *ACS Catalysis*, **2017**, 7 (4), 2346-2352.

34. Musić, S.; Popović, S.; Maljković, M.; Skoko, Z.; Furić, K.; Gajović, A. Thermochemical formation of IrO_2 and Ir, *Materials Letters*, **2003**, *57* (29), 4509-4514.

35. Audichon, T.; Guenot, B.; Baranton, S.; Cretin, M.; Lamy, C.; Coutanceau, C. Preparation and characterization of supported $Ru_xIr_{(1-x)}O_2$ nano-oxides using a modified polyol synthesis assisted by microwave activation for energy storage applications, *Applied Catalysis B: Environmental*, **2017**, *200*, 493-502.

36. Liao, P. C.; Chen, C. S.; Ho, W. S.; Huang, Y. S.; Tiong, K. K. Characterization of IrO_2 thin films by Raman spectroscopy, *Thin Solid Films*, **1997**, *301* (1), 7-11.

37. Zeradjanin, A. R.; Topalov, A. A.; Van Overmeere, Q.; Cherevko, S.; Chen, X.; Ventosa, E.; Schuhmannc, W.; Mayrhofer, K. J. J. Rational design of the electrode morphology for oxygen evolution - enhancing the performance for catalytic water oxidation, *RSC Advances*, **2014**, *4* (19), 9579-9587.

38. Willinger, E.; Massué, C.; Schlögl, R.; Willinger, M. G. Identifying Key Structural Features of IrO_x Water Splitting Catalysts, *Journal of the American Chemical Society*, **2017**, 139 (34), 12093-12101.

39. Trasatti, S.; Buzzanca, G. Ruthenium dioxide: A new interesting electrode material. Solid state structure and electrochemical behaviour, *Journal of Electroanalytical Chemistry and Interfacial Electrochemistry*, **1971**, *29* (2), A1-A5.

40. Kahk, J. M.; Poll, C. G.; Oropeza, F. E.; Ablett, J. M.; Céolin, D.; Rueff, J. P.; Agrestini, S.; Utsumi, Y.; Tsuei, K. D.; Liao, Y. F.; Borgatti, F.; Panaccione, G.; Regoutz, A.; Egdell, R. G.; Morgan, B. J.; Scanlon, D. O.; Payne, D. J. Understanding the Electronic Structure of IrO_2 Using Hard-X-ray Photoelectron Spectroscopy and Density-Functional Theory, *Physical Review Letters*, **2014**, *112* (11), 117601.

41. Panda, S. K.; Bhowal, S.; Delin, A.; Eriksson, O.; Dasgupta, I. Effect of spin orbit coupling and Hubbard *U* on the electronic structure of IrO_2, *Physical Review B*, **2014**, *89* (15), 155102-155107.

42. Cruz, A. M.; Abad, L.; Carretero, N. M.; Moral-Vico, J.; Fraxedas, J.; Lozano, P.; Subías, G.; Padial, V.; Carballo, M.; Collazos-Castro, J. E.; Casañ-Pastor, N. Iridium Oxohydroxide, a Significant Member in the Family of Iridium Oxides. Stoichiometry, Characterization, and Implications in Bioelectrodes, *The Journal of Physical Chemistry C*, **2012**, *116* (8), 5155-5168.

43. Chakthranont, P.; Kibsgaard, J.; Gallo, A.; Park, J.; Mitani, M.; Sokaras, D.; Kroll, T.; Sinclair, R.; Mogensen, M. B.; Jaramillo, T. F. Effects of Gold Substrates on the Intrinsic and Extrinsic Activity of High-Loading Nickel-Based Oxyhydroxide Oxygen Evolution Catalysts, *ACS Catalysis*, **2017**, 7 (8), 5399-5409.

44. Ng, J. W. D.; García-Melchor, M.; Bajdich, M.; Chakthranont, P.; Kirk, C.; Vojvodic, A.; Jaramillo, T. F. Gold-supported cerium-doped NiO_x catalysts for water oxidation, *Nature Energy*, **2016**, 1, 1-8.

Figures
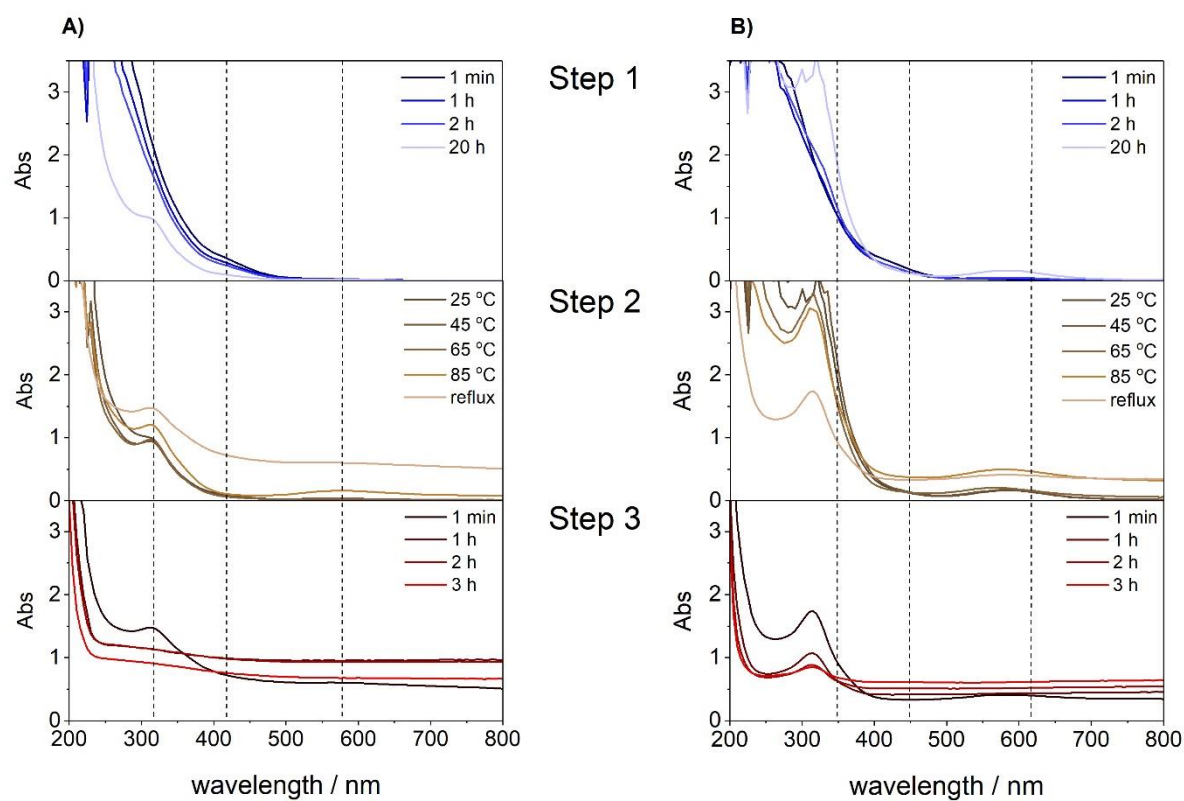
Figure 1. UV-Vis monitoring during step 1 (stirring at 25 °C for 20 h), step 2 (heat from 25 °C to reflux) and step 3 (reflux for 3 h) of the hydrothermal conversion of $IrCl_3$ to IrO_2 using a) Li_2CO_3 and b) LiOH as a base.
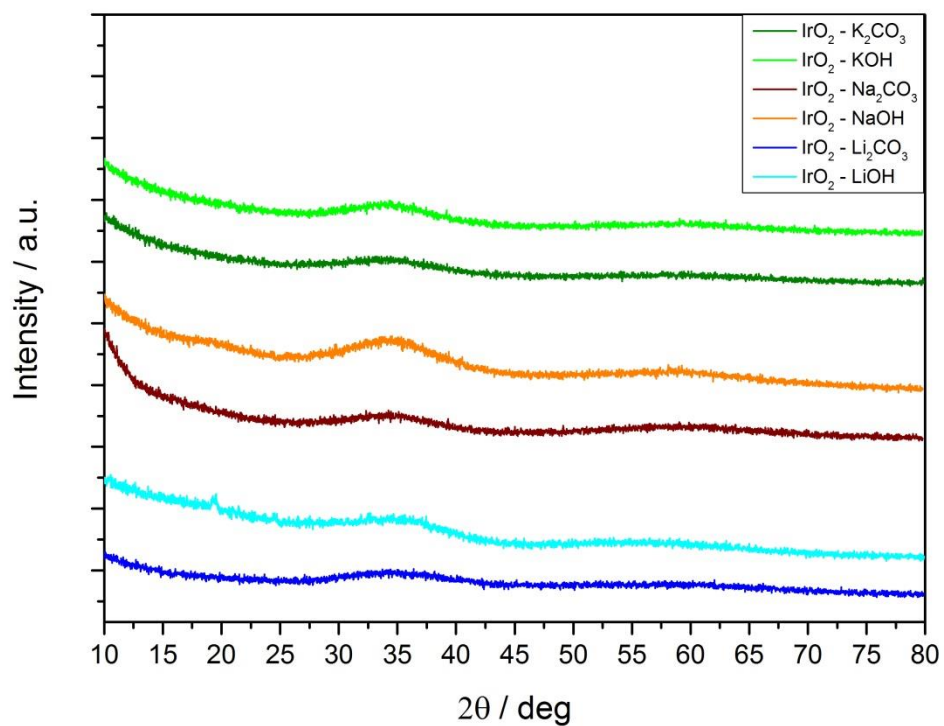
Figure 2. XRD patterns for hydrothermally prepared IrOx catalysts using different bases.
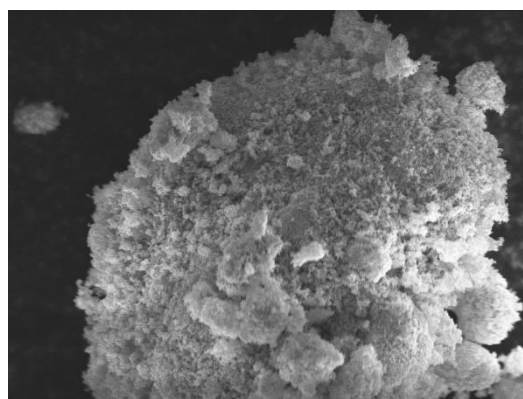

5 µm IrOₓ-Li₂CO₃

5 µm IrOₓ-LiOH
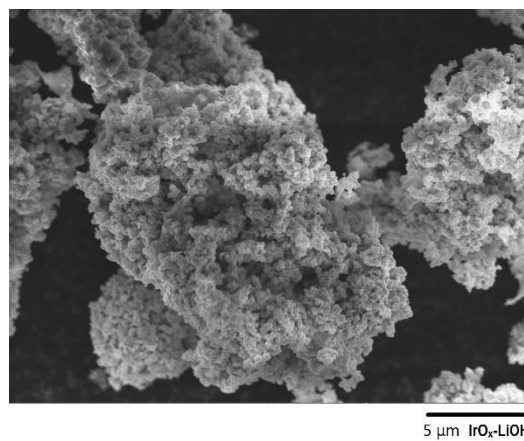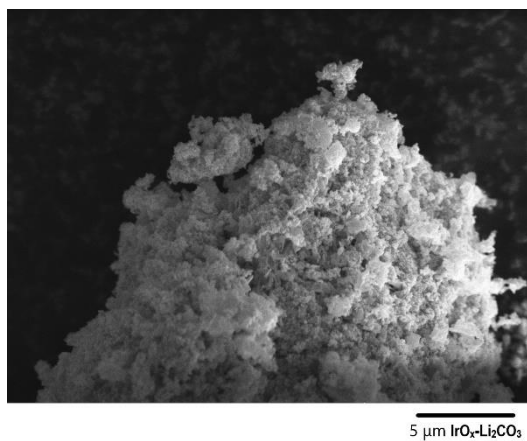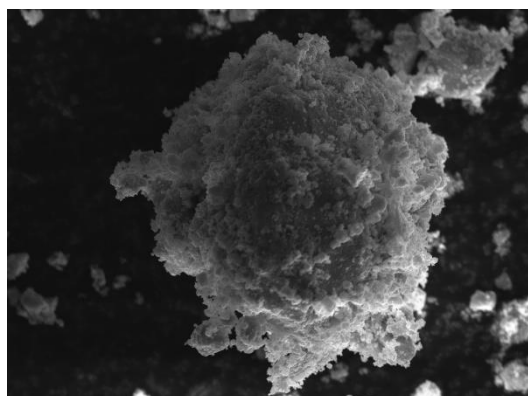
5 μm IrOx-Na2CO3
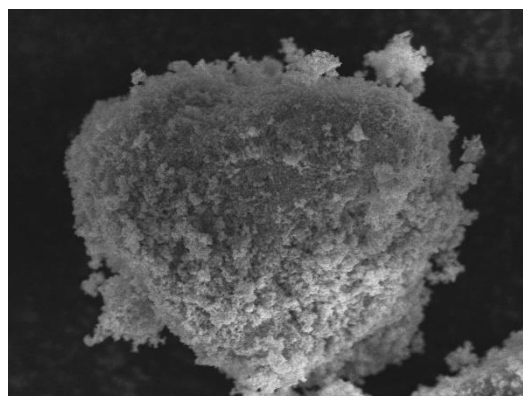
5 μm IrOx-NaOH
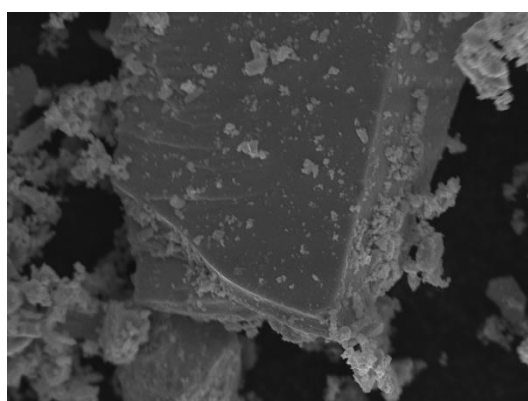
5 μm IrOx-K2CO3
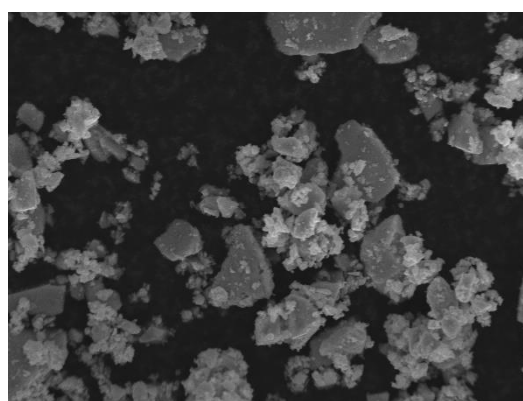
5 μm IrOx-KOH
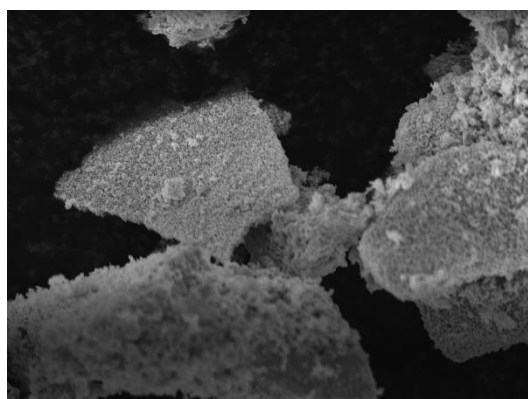
5 μm IrO2-SA

5 μm IrOx-AA

Figure 3. SEM images for IrOx-base catalysts hydrothermally prepared.
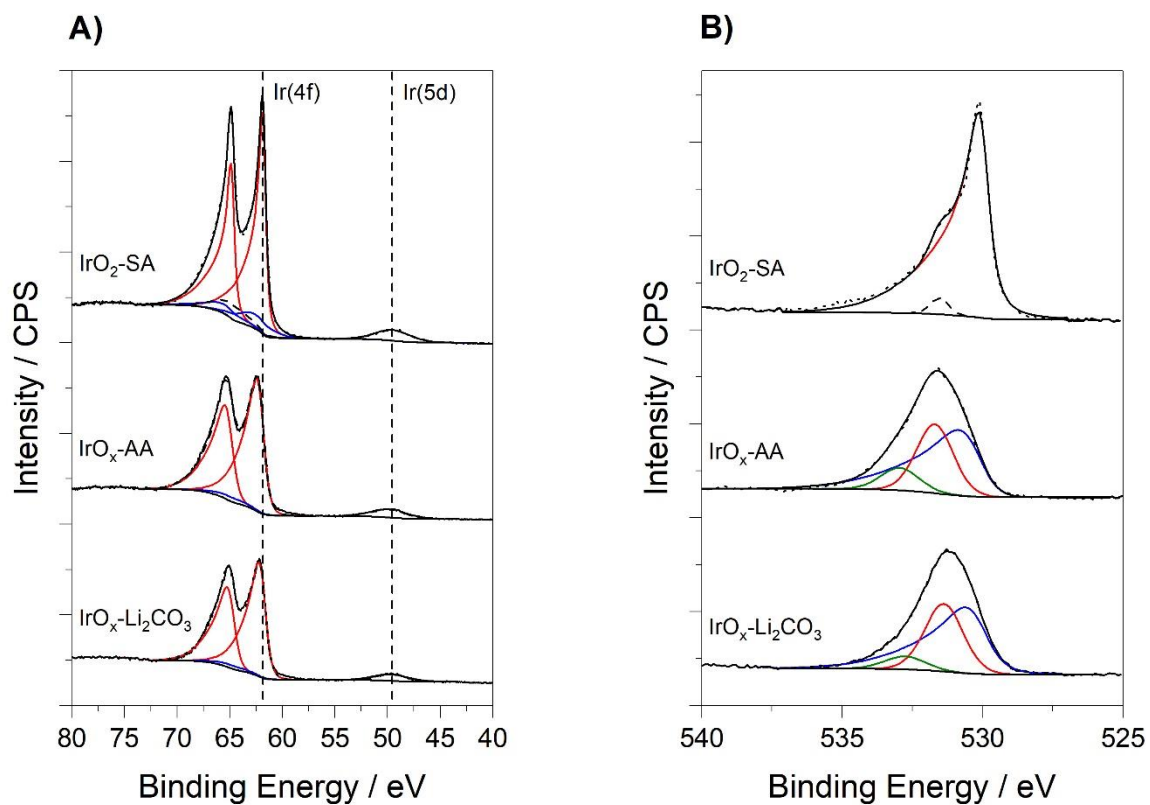
Figure 4. a) Ir(4f) and b) O(1s) XPS line fitting for commercial rutile IrO_2-SA and amorphous IrO_x-AA compared to hydrothermally synthesised IrO_x-Li_2CO_3. In the Ir(4f) region, the Ir(4f) and the Ir(5p) are represented in red and blue respectively. In the O(1s) region, oxide, hydroxide and water/carbonate are represented in red, blue and green respectively.
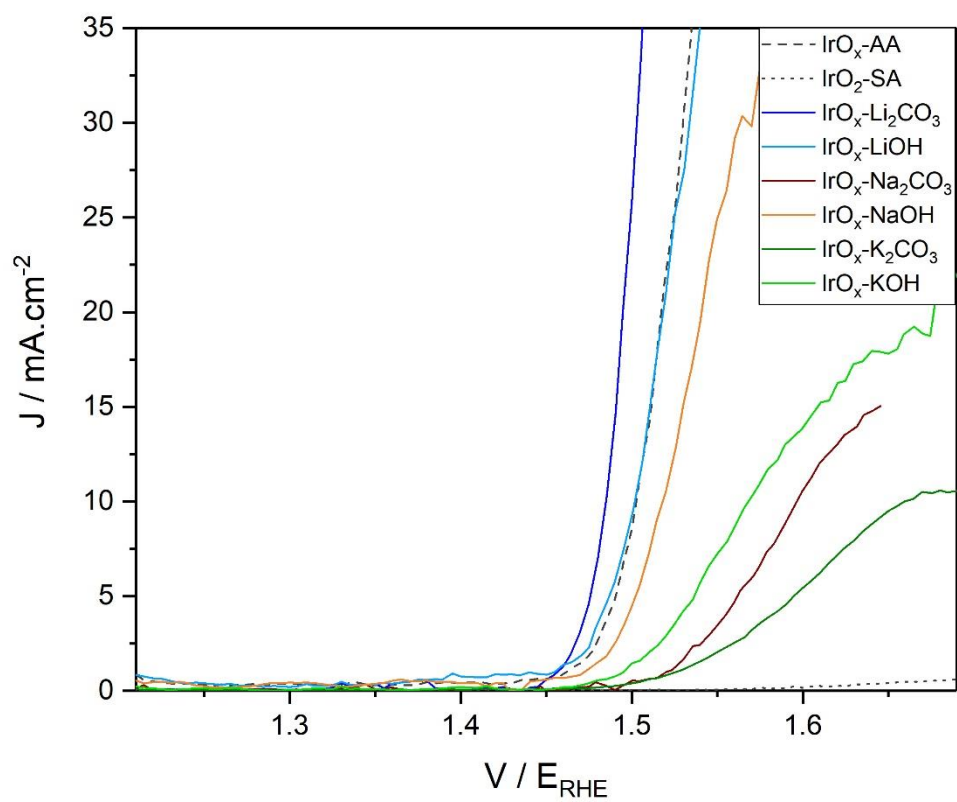
Figure 5. Catalytic intrinsic activity of commercial IrO_2 standards and hydrothermally prepared IrO_x catalysts determined by LSV (1.2 V_{RHE} to 1.7 V_{RHE} at 5 mV·s⁻¹).

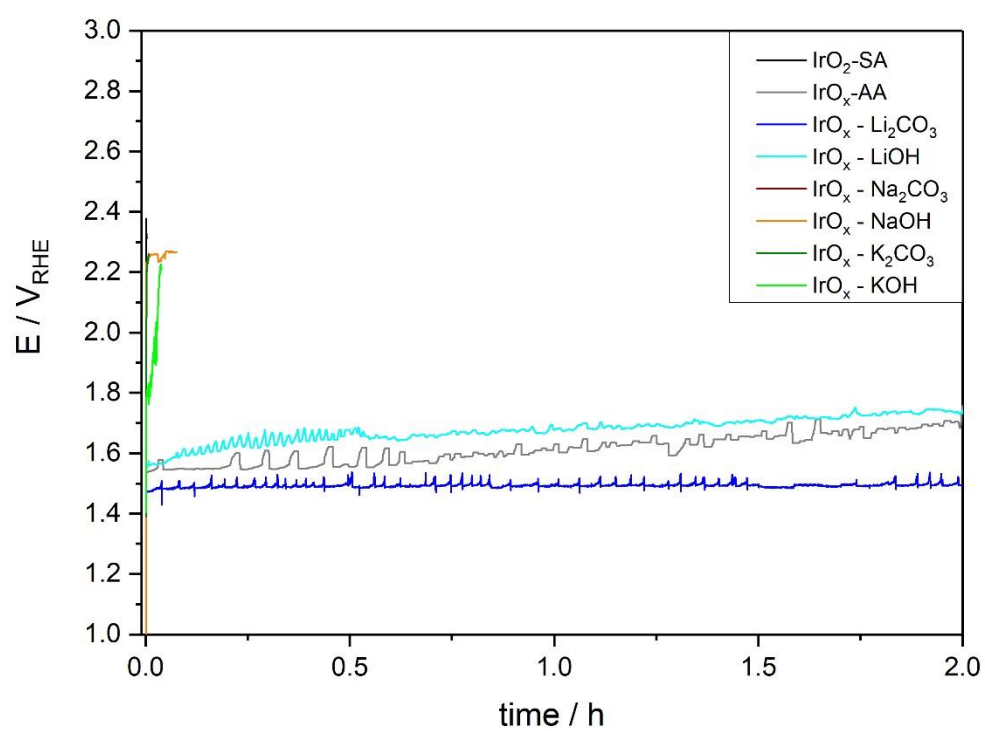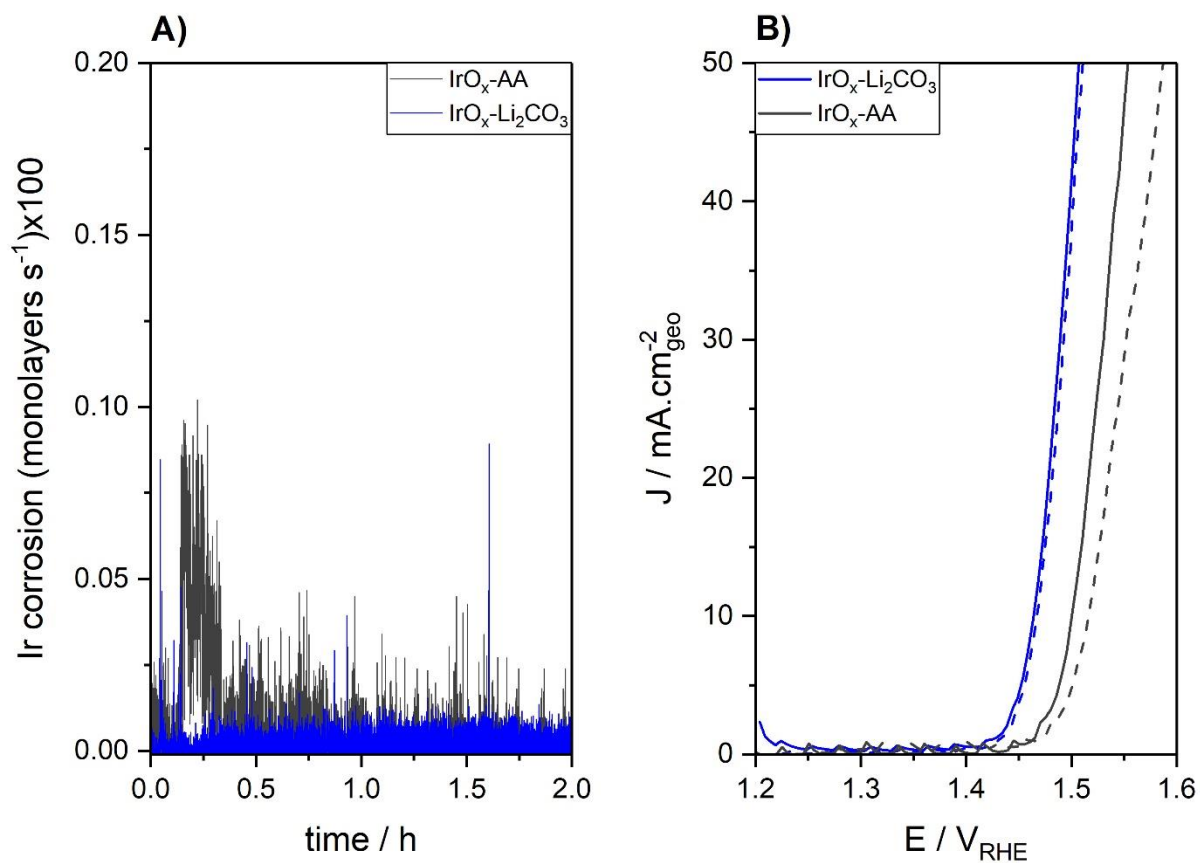**Figure 6.** Assessment of catalyst stability via chronopotentiometry (2 h at 10 mA·cm^{-2}).

Figure 7. a) iridium dissolution monitored by ICP-coupled to the electrochemical flow cell during CP (10 mA·cm^{-2}, 2 h) and b) LSV measurement recorded before (solid line) and after (dashed line) the CP measurement.

Tables

Table 1. BET surface area of hydrothermally prepared catalysts using different bases.

Catalyst	BET surface area m²/g$_{cat}$	catalyst	BET surface area m²/g$_{cat}$
IrO_2-SA	2	IrO_x-AA	33
IrO_x-LiOH	10	IrO_x-Li_2CO_3	35
IrO_x-NaOH	3	IrO_x-Na_2CO_3	3
IrO_x-KOH	1	IrO_x-K_2CO_3	1

Table 2. XPS derived relative oxygen speciation (oxide, hydroxide and water/carbonate) obtained from the O(1s) peak fitting.

catalyst	O - oxide / %	O - hydroxide / %	O - water/CO_3^{2-} / %
IrO_2-SA	100	0	0
IrO_x-AA	56	33	11
IrO_x-Li_2CO_3	57	36	7
IrO_x-LiOH	53	37	10
IrO_x-Na_2CO_3	71	24	5
IrO_x-NaOH	84	12	4
IrO_x-K_2CO_3	64	31	5
IrO_x-KOH	70	23	7

Table of contents graphic (TOC)